

Chapter 7

Ionization of uracil and bromouracil : keV energy protons vs MeV energy HCIs

7.1 Introduction

Interaction of ionizing radiation with biological matter leads to structural and chemical modifications in the cells resulting in the mutation of genes finally causing cell death. Single and double strand breaks of the DNA/RNA caused mostly by the secondary particles like low energy electrons, ions and free radicals which are produced during direct ionization are the main causes of radiation damage [171]. In hadron therapy, protons and highly charged ions are used for treating the malignant cells. The use of ions for treating tumours itself is beneficial compared to other modes of radiation due to the presence of the Bragg peak which can be exploited fully by overlapping the peak position at the tumour location. At the Bragg peak region, the incoming ion beam gives off almost all its energy to the target medium and then comes to rest. This phenomena leads to precise deposition of dose mostly to the tumour cells, although several healthy cells along with the tumour cells are also affected, which causes significant side effects for the patients. This led to the need for targeted drugs which can increase the killing of tumour cells and reduce the damage to surrounding healthy cells. Radiosensitizers are such a modality that enhances the lethal effects of radiation especially on the malignant cells compared to the normal cells, i.e., enhance tumour cell killing with negligible effect on surrounding normal cells [172, 173]. Thus hadron therapy which has the advantage of precise dose deposition when combined with radiosensitizers can be used as an effective mode for cancer treatment. The addition of a high- Z atom loaded compound is considered as an elegant method for enhancing the effect of ionizing radiation. In this regard, metal nanoparticles made of gold, platinum, gadolinium have already been investigated [50, 174, 175, 176, 177, 178]. To increase the radiosensitization effect, the nanoparticles are targeted directly to the tumour cells. The presence of the nanoparticles loaded with high- Z atom increases the absorption of ionizing radiation which leads to the production of additional low energy electrons around the DNA. In such studies, the ratio of strand breaks (single and double) in the presence and absence of nanoparticles are obtained experimentally. It has been observed that there is substantial increase in the strand breaks in the presence of the nanoparticles. Some of the studies were focussed on understanding the difference in the nature of breakage when caused by pure nanoparticle clusters and when the nanoparticles are attached to other ligands to form a compound of the same. In this direction, halouracils are also well known for exhibiting

radiosensitizing effects [52]. The class of 5-halouracil molecules ($C_4H_3XN_2O_2$, $X = F, Cl, Br, I$) are structurally similar to uracil ($C_4H_4N_2O_2$), one of the nucleobase of RNA. Bromouracil ($C_4H_3BrN_2O_2$) is obtained by replacing the H atom at the 5th position of uracil by a Br atom. Several experimental and theoretical studies have been undertaken in the recent past on bromouracil and other halouracils in their gas phase as well as in cluster forms [179, 180, 181, 47, 182]. In this chapter we present the DDCS of electron emission from uracil and bromouracil in collisions with keV energy protons and MeV energy bare C ions. The measured results were compared with the CDW-EIS calculations. Further, from the present measurements we aim to provide an estimate of enhancement in electron production from bromouracil compared to uracil when ionized by the same projectile beam. Such a quantitative estimate can serve as a solid input towards the radiosensitizing property of bromouracil.

7.2 Experimental details

The experimental techniques have already been discussed in details in chapter 2. A brief description of the target preparation and data collection technique for vapour target are discussed here. The bromouracil (BrU) powder was placed inside the metallic oven and heated gradually over a period of approximately 24 hrs. The rate of flow of the BrU vapour effusing out of the jet was monitored continuously with the help of the quartz crystal based thickness monitor. Before the vapour starts coming out, the background spectra were collected for all the emission angles. The data were collected for a particular rate of flow of the vapour. This flow rate was ascertained based on three factors : i) the count rate was several times above background counts ii) the flow rate remained steady over substantial period of time iii) rate should not be so high that it forbids single collision condition. It is to be noted here that with the passage of time the BrU vapour starts depositing on the walls of the chamber and on the plates of the spectrometer and collimator. The deposition on the collimator and front plate of the spectrometer gives rise to local field effects near the interaction region which eventually causes hindrance to the accurate collection of the low energy electrons. This problem was circumvented by collecting the data initially upto 100 eV for all the emission angles at a relatively lower effusing rate (i.e., before there is substantial deposition on the collimator and spectrometer plates) of approximately 0.2 angstrom/sec. Further, the flow rate was increased for collecting data for higher energy electrons, since the count rate decreases with the increase in emission energy. For higher electron energies, the rate was fixed at around 0.6 - 0.7 angstrom/sec. After increasing the rate, data were collected only after ensuring that the rate was stable for several hours. The entire process of heating the powder was done very slowly, i.e., at every instant the temperature was increased in small step and the rate of flow of the vapour was allowed to settle accordingly before any further increase of temperature. This method had to be followed, otherwise, fast heating would either blow out the entire powder in the container or due to poor thermal conductivity of the

powder material, the heat would not be transferred uniformly which could clog the jet nozzle, preventing the vapour from coming out of the nozzle completely. To generate uniform heating of the target powder inside the container, a copper rod was designed and prepared, which would be attached at the bottom of the container such that it would be in direct contact with the metal oven. Figure 7.1 shows the 3D mechanical drawing of the interaction region where the ion beam collides with the BrU vapour coming out of the jet nozzle along with the cut view of the spectrometer analyzing the electrons ejected from the target molecule. The nozzle tip was kept 5 mm below the beamline and before data collection it was ensured that the beam was not hitting any part of the target holder assembly of the nozzle tip which would otherwise give rise to huge background counts. The first part of the experiment was performed with 66 MeV bare C ions obtained from the 14 MV Pelletron accelerator. The data were collected over a wide angular range from 20° to 160° . After performing the experiment with BrU, the chamber walls and spectrometer plates were cleaned and then under the same experimental conditions data were collected for uracil with the same projectile beam. In case of BrU, measurements were also performed for 42 MeV bare C ions. The aspect ratio (diameter/length) of the nozzle that was used for the present series of experiments was 0.1.

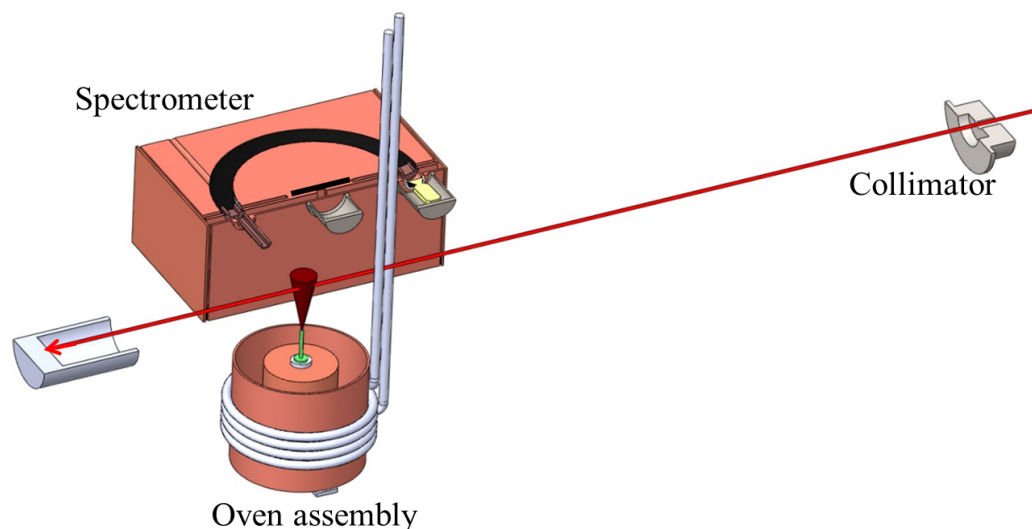


Figure 7.1: 3D schematic diagram of ion beam interacting with the vapour target effusing from the jet nozzle placed above the metallic oven (made using Solidworks 2014).

Further the investigations were extended towards the lower energy ions. For this purpose, the ECR ion accelerator was used to produce the 200 keV protons. In this case also, the measurements were performed initially for bromouracil and then for uracil under the same conditions. The jet nozzle was aligned with respect to the beamline by performing mechanical alignment initially and then by checking the count rate in beam “ON” condition. Further de-

tails on the alignment is explained in chapter 2. In this case the aspect ratio of the nozzle was 0.125 and was placed 5 mm below the beamline. The data were collected for 10 different angles namely, 20° , 30° , 45° , 60° , 75° , 90° , 105° , 120° , 135° , 150° .

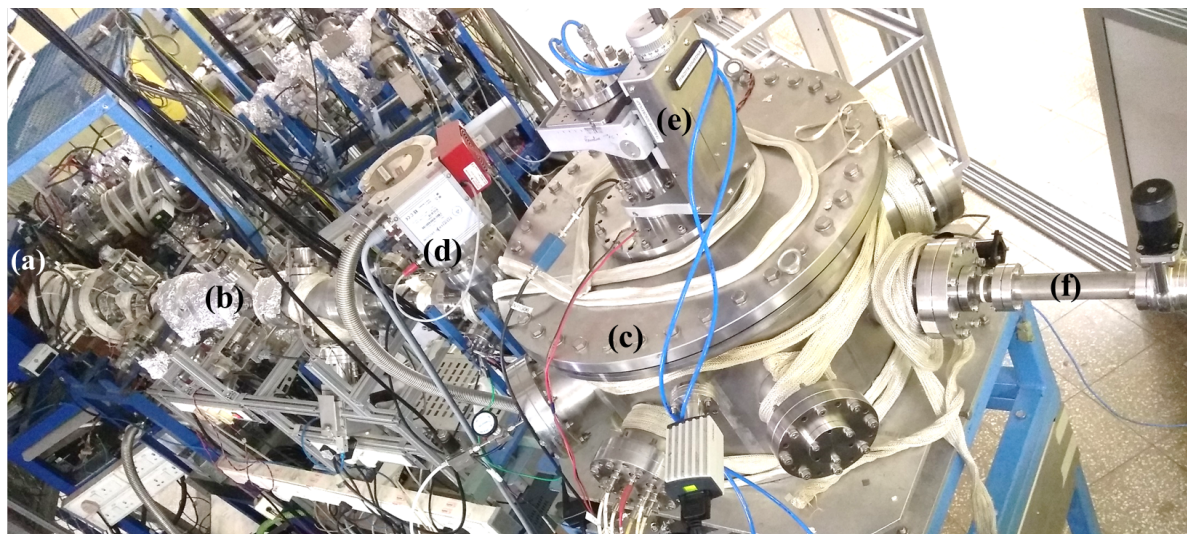


Figure 7.2: Electron spectroscopy setup at ECRIA : (a) Switching magnet (b) 50° N beamline of ECR ion accelerator (c) Scattering chamber housing the electron spectrometer (d) differential pumping assembly (e) 3D translation stage manipulator holding the oven assembly, blue tubing are for water flow to the jacket surrounding the oven (f) Faraday Cup, electrically isolated from the scattering chamber.

7.3 Absolute normalization of DDCS spectra

In order to determine the absolute values of the e-DDCS, it is important to determine the exact number of target molecules at the interaction region. It is difficult to obtain the reliable number density for an effusive jet target. To circumvent this problem, a novel method is used to obtain the electron DDCS in the absolute scale. At the first step, DDCS measurements were performed for O_2 gas target to obtain the absolute total K-LL Auger electron emission cross-section for an O-atom. This measurement was performed with a static pressure condition, so that, the gas density was known exactly and then the DDCS was determined from the first principle, as already described in chapter 2. Then, further integrating the DDCS over peak energy and the angles one can get the total K-LL Auger cross section for O-atom.

$$\sigma_{abs}(O - KLL, O_2) = \int \int_{Auger} \left(\frac{d^2\sigma}{d\epsilon d\Omega} \right) d\epsilon d\Omega \quad (7.1)$$

In the second step, the relative DDCS for the biomolecules, uracil and bromouracil were determined in case of the effusive jet experiment. For each angle, the DDCS spectrum was corrected for the solid angle-path length integral convoluted with with the molecular jet density

profile which is given as :

$$\frac{d^2\sigma}{d\epsilon d\Omega} = \frac{\frac{N_e(\epsilon, \theta)}{N_p \Delta\epsilon} - \frac{N_b(\epsilon, \theta)}{N'_p \Delta\epsilon}}{\epsilon_{el}(l\Omega)_{eff} j(\theta)} \quad (7.2)$$

where $j(\theta)$ is the vapour density relation due to the jet geometry, (see chapter 2). Then the relative single differential cross-section ($\frac{d\sigma_{rel}}{d\epsilon}$) was calculated by integrating the DDCCS over the emission angle. Integrating the SDCS further over the K-LL Auger peak for oxygen from bromouracil, one can get the total (relative) K-LL Auger cross section for O atom from bromouracil.

$$\sigma_{rel}(O - KLL, BrU) = \int \int_{Auger} \left(\frac{d^2\sigma}{d\epsilon d\Omega} \right) d\epsilon d\Omega \quad (7.3)$$

Since the K-LL Auger emission is an inner-shell process, in the normalization procedure, it was assumed that the contribution of K-LL Auger cross-section per O-atom of bromouracil ($C_4H_3BrN_2O_2$) molecule is equal to that for the O-atom in an O_2 molecule. From this condition, the normalization factor is obtained as :

$$N = \frac{\sigma_{abs}(O - KLL, O_2) \times n_O}{\sigma_{rel}(O - KLL, BrU)} \quad (7.4)$$

where n_O is the number of oxygen atoms in BrU. Thus the absolute DDCCS is then obtained from the relative DDCCS by multiplying by the normalization factor N , such that :

$$DDCS_{abs} = DDCCS_{rel} \times N \quad (7.5)$$

The absolute DDCCS for electron emission from uracil were also obtained in the similar manner. The total uncertainty in the present measurements was estimated to be around 25%.

7.4 Ionization of biomolecules by MeV energy bare C ions

7.4.1 Energy distribution of electron DDCCS

Figure 7.3 and Figure 7.4 display the absolute DDCCS for electron emission from bromouracil and uracil in collisions with 66 MeV C^{6+} ions. The data have been shown for different forward and backward emission angles. In each case the data are shown for electron energies from few eV to 620 eV. The cross section shows a maximum value for the lowest energy electrons, due to the soft collision effect. These low energy electrons are the key factors for strand breaks. The intermediate part of the spectrum is governed by the two center effect. In case of two center effect, the ejected electron is under the influence of two centers, i.e., the pro-

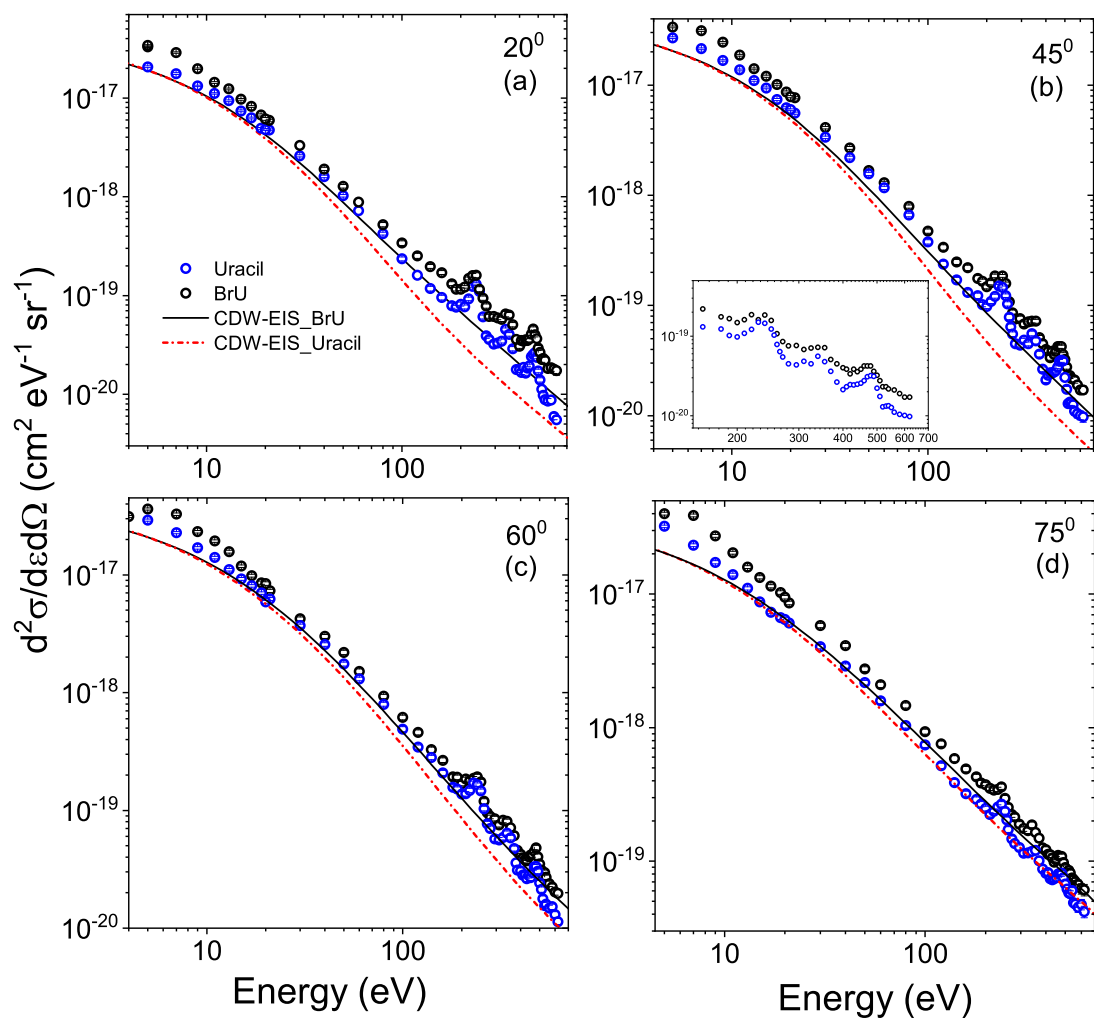


Figure 7.3: Absolute electron DDCS at fixed emission angles for 66 MeV C^{6+} ion impact on bromouracil (black open circles) and uracil (blue open circles). The black solid and red dash-dotted lines correspond to the CDW-EIS calculations for bromouracil and uracil, respectively. Inset of (b) : magnified view of the K-LL Auger lines for C, N and O.

jectile center and the target ion center. The emitted electrons experience a forward pull along the direction of the projectile which are highly charged ions in the present case. Due to this phenomena, the cross sections are higher at forward angles compared to the complementary backward angles, giving rise to the forward-backward angular asymmetry which will be discussed at a later stage in this chapter. Beyond 200 eV, three peak like structures can be seen at each and every spectrum. These three peaks represent the K-LL Auger characteristic lines for carbon, nitrogen and oxygen. The Auger line for carbon is seen around 240 eV, whereas those for nitrogen and oxygen are visible at about 350 eV and 480 eV, respectively. The Auger lines are prominent mostly in the forward and backward angles. In case of the intermediate angles, around 90° , due to the dominance of the binary encounter mechanism, the peaks are not

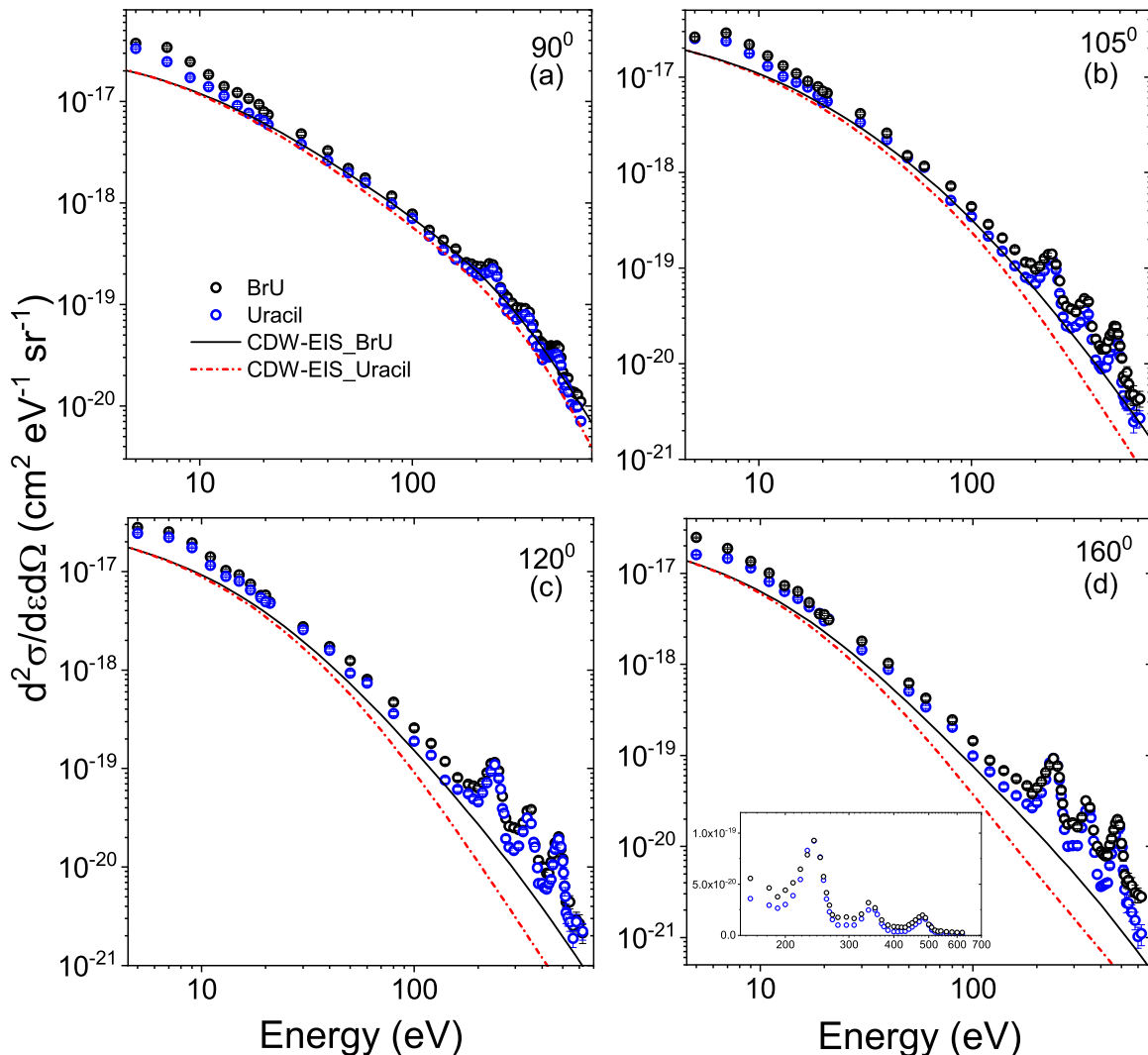


Figure 7.4: Same as Figure 7.3, except for different emission angles.

seen very prominently. The inset of Figure 7.3(b) shows the magnified view of the three K-LL Auger lines seen in the DDCS spectra for uracil (blue circles) and bromouracil (black circles). The experimentally measured DDCS for uracil and bromouracil have been compared with the prior version of the CDW-EIS model. The CDW-EIS calculations are shown by the black solid lines for bromouracil and red dash-dotted lines for uracil. The molecular structure of the bromouracil and uracil molecules are determined at the restricted Hartree-Fock (RHF)/3-21G level of theory with geometrical optimization using the Gaussian 09 software. The effective occupation analysis of the differential cross-sections for each molecular orbital is performed using the complete neglect of differential overlap (CNDO) approximation. In this approximation, the representation of the molecular orbitals is reduced to a one-center linear combination of their atomic compounds, neglecting, as above mentioned, all terms corresponding to the overlap of the atomic states. This description is expected to be valid assuming that we deal with the target

molecules averaged over their entire space orientations and hence a one-center image may be considered as reasonable. Thus the differential cross section for each orbital was obtained as a sum of the corresponding atomic compounds. In case of the forward angles in [Figure 7.3](#), it is seen that the CDW-EIS calculations underestimate the experimental measurements for both uracil and bromouracil. For the lowest electron energies, the calculations for uracil are in close agreement with the data points, however, the deviation increases with the increase in emission energies. It is further noticed that the calculations for uracil and bromouracil almost merge together upto around 20 eV, beyond with the cross section for uracil are lower than that for bromouracil. For 75° ([Figure 7.3\(d\)](#)) and 90° ([Figure 7.4\(a\)](#)), the CDW-EIS predictions match well with the experimentally measured DDCS for uracil over the entire emission energy except for the low energy electrons below 20 eV. In this region, the measured DDCS are seen to be higher than the calculations. At the backward angles, the theoretical calculations for uracil underestimate the data over the entire energy range measured in the present experiments. In case of bromouracil it is observed that theory underestimates the data for all the emission angles. Although the CDW-EIS predictions are lower than the data points for bromouracil for all the cases, maximum discrepancy is observed for the forward and backward emission angles. Similar to the case observed for uracil, around 90° , the calculated cross section for bromouracil are close to the measured DDCS spectra although quantitatively are lower than the measured data. In the inset of [Figure 7.4\(d\)](#), the Auger lines for C, N and O are plotted in the log-linear scale. The higher yield for the C-Auger peak (~ 240 eV) is due to the contribution from the four carbon atoms in uracil or bromouracil whereas the other characteristic peaks are due to the presence of two atoms each of nitrogen and oxygen.

Similarly, in [Figure 7.5](#) we have shown the DDCS for electron emission from bromouracil upon impact by 42 MeV bare C ions. The data are shown for six different emission angles and are further compared with the CDW-EIS calculations which are shown by the red dash-dotted lines. The measured DDCS are reproduced well by the model predictions. Qualitatively an excellent agreement is observed between the calculated and measured DDCS. However, quantitatively it is seen that the CDW-EIS predictions underestimate the data for all the emission angles. The difference is least in case of 75° , whereas it increases while moving towards the extreme forward and backward angles. The uncertainties due to counting statistics were quite small, being within the symbol size and hence are not visible except for few points in [Figure 7.5\(f\)](#) around 1000 eV. The count rate being quite less in this region, the statistical error bars are seen in the spectrum. The data were collected upto 1500 eV to include the L-MM Auger line of Br. A magnified view of this L-MM Auger peak of Br is shown in the inset of [Figure 7.5\(f\)](#). Similarly, the K-LL Auger lines due to the presence of carbon, nitrogen and oxygen in bromouracil are shown in the inset of [Figure 7.5\(e\)](#).

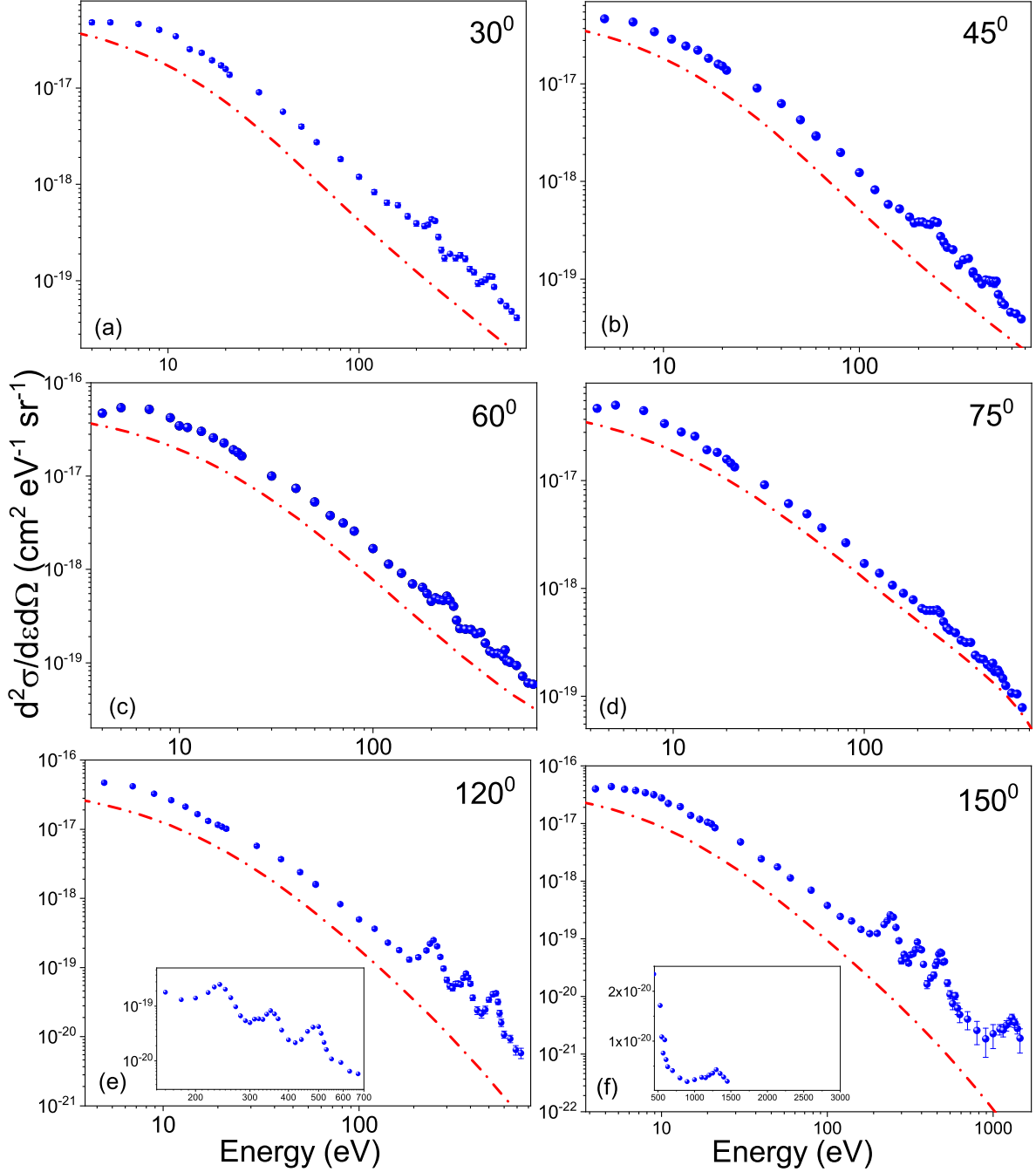


Figure 7.5: Absolute electron DDCS at fixed emission angles for 42 MeV C^{6+} ion impact on bromouracil. The red dash-dotted lines correspond to the CDW-EIS calculations for bromouracil. Inset of (e) : magnified view of the K-LL Auger lines for C, N and O, inset of (f) : L-MM Auger peak of Br.

7.4.2 DDCS ratios between bromouracil and uracil

From Figure 7.3 and Figure 7.4, in the log-log scale it is difficult to understand the exact difference in cross section between the two targets. In Figure 7.6 we have shown the ratio of the electron DDCS from bromouracil to uracil as a function of electron emission energy. The

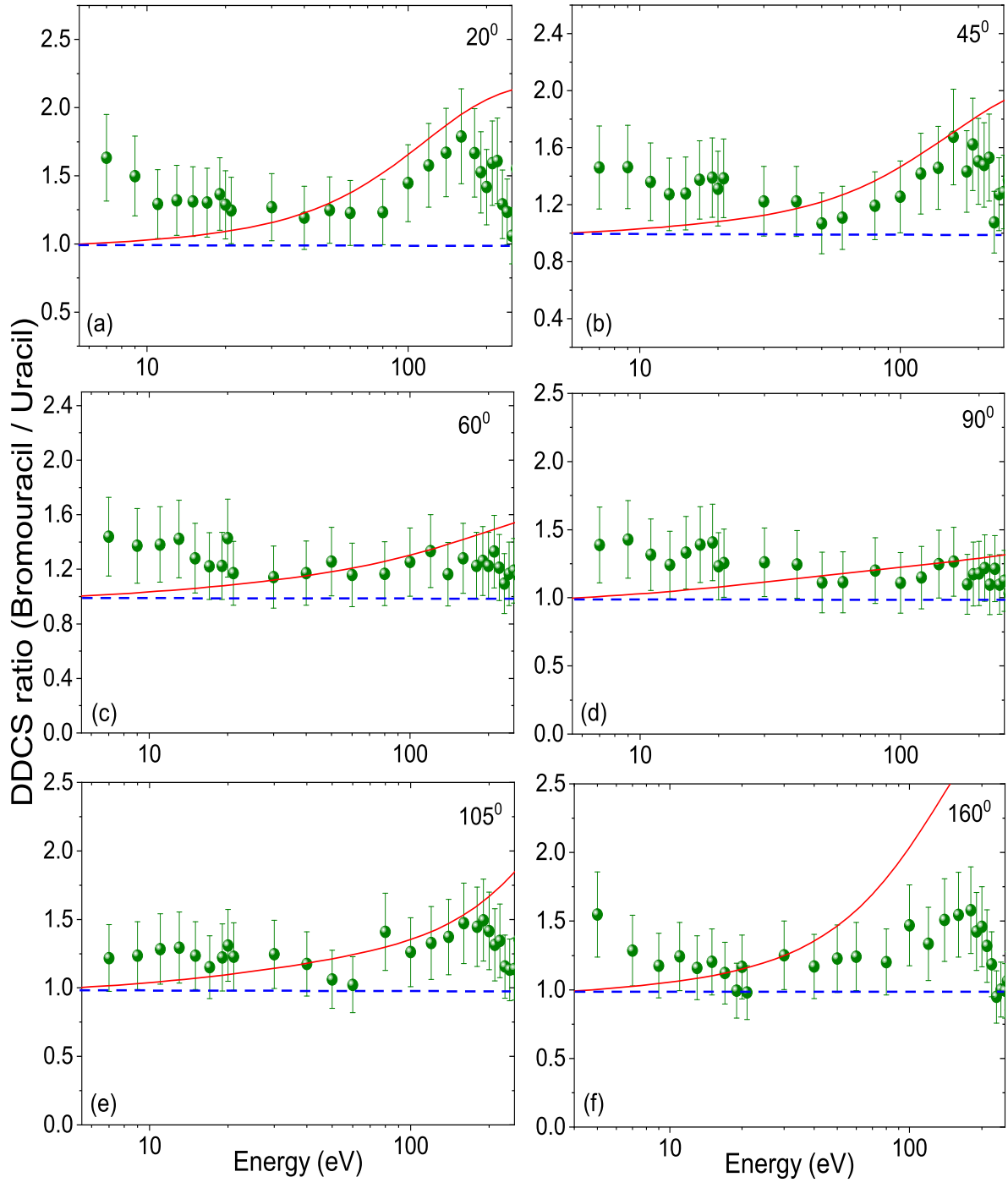


Figure 7.6: Ratio of DDCS between bromouracil and uracil for different emission angles; Projectile : 66 MeV bare C ions. The red solid line shows the DDCS ratio from the CDW-EIS predictions, whereas the blue dashed line represent the ratio value at 1.0.

DDCS ratios have been plotted for six different forward and backward emission angles. The ratios have been shown for emission energies between 5 eV and 250 eV. From these ratios one can get a clear estimate of the increase in cross section from bromouracil compared to uracil. It is seen that an overall enhancement of ~ 1.25 times is obtained for all the emission angles. The

blue dashed line represents the DDCS ratios at 1.0. The ratios obtained from the theoretically calculated DDCS of bromouracil to uracil are seen to match with the experimental ratios beyond 30 eV for majority of the emission angles. For the lowest electron energies plotted here, i.e., 5 eV and above, the theoretical ratios are 1.0 and then gradually rises and merges with the experimental ratios at 30 eV and above (within experimental uncertainties). It is to be noted that the low energy electrons of 1 to 30 eV are the most favourable candidates for the present purpose related to hadron therapy. In case of 160° emission angle (see [Figure 7.6\(f\)](#)), the DDCS ratios obtained from the CDW-EIS calculations showed a sharp increase with the emission energy, although any physical significance for the same is not known. The enhancement by a factor of 1.25 times deduced from the experimentally measured DDCS ratios is not explained accurately by the CDW-EIS model which takes into account the contribution of single ionization arising from all the 29 orbitals for uracil and the 46 orbitals for bromouracil. According to the model predictions, in the low energy regime, i.e., where the soft collision mechanism is predominant, the contribution due to Coulomb ionization is the same for either molecules irrespective of the number of electrons present in each molecule. It thus appears that along with single ionization some other mechanism is also involved which shows the increase in electron emission yield in the low energy region. This enhancement in the ratio of cross sections for bromouracil to uracil may be explained by the Auger cascade mechanism which is caused due to a vacancy created in an inner shell of the high-Z atom and subsequently several other vacancies are created in the outer shells leading to multiple electrons being emitted simultaneously. Further, the electrons in the $3d$ subshell of Br may also contribute to the atomic giant dipole resonance (GDR). In this phenomena, the $3d$ electrons decay by the emission of several low energy electrons, which can in turn contribute to the ionization cross section for BrU. The DDCS ratios based on the present measurements suggest that the inclusion of the Br atom to uracil increases the yield of electron production by 1.25 times.

7.5 Ionization of biomolecules by keV energy protons

It is well known that carbon ions and protons are the two most favourable candidates for hadron therapy. In case of protons, the energy loss at the Bragg peak is not as sharp as that for carbon ions. Further, it is important to note that at the end of the ion track, i.e., at macroscopic distances beyond the Bragg peak, the primary ion beam still bearing its remaining energy of several hundreds of eV gives off the energy to the surrounding biological media [183]. As a result healthy cells which are located beyond the tumour volume are also affected. For heavy ions this phenomena is more prevalent, whereas for protons, the dose deposition profile beyond the Bragg peak is negligible [32]. We have extended the present investigations from heavy ions to protons with keV energy. This study was aimed to understand the change in behaviour of the

low energy electron emission from the nucleobase and its halogenated derivative along with studying the enhancement in electron emission (if any) by reducing the beam energy and also changing the projectile species. For this purpose, experiments were performed for 200 keV protons colliding with uracil and bromouracil.

7.5.1 Energy distribution of electron DDCS

Figure 7.7 displays the energy distribution of the DDCS spectra for six different emission angles, namely, 20° , 45° , 60° , 90° , 105° and 150° . The shape of the spectra at the forward and backward emission angles are slightly different than that seen in Figure 7.3 and Figure 7.4. A close look at the spectra for the low forward angles shows that the characteristic K-LL Auger lines for C, N and O atoms are not visible unlike that seen in Figure 7.3. For the MeV energy highly charged ions (HCIs), there is a sharp fall in the DDCS spectra with increase in emission energy, however, in the present case it is seen that along with the fall in the DDCS spectra, a hump like structure is observed around 300 eV in Figure 7.7(a). It is further noticed that with the increase in emission angle, the position of the hump shifts towards the lower emission energies. This hump exhibits the binary collision mechanism. Ideally the binary collision is expected to give rise to a prominent peak in the DDCS spectrum, but due to the initial momentum distribution of the electron bound to the target molecule orbital, the peak is spread out. The projectile velocity being close to the orbital electron velocities, the post collision effect is very strong for the present beam. Due to the large outer shell ionization contribution, the characteristic Auger lines are not visible in the forward angles. In case of 90° and above, the K-LL Auger lines are seen for both the target molecules uracil and bromouracil. The peaks at 240 eV, 350 eV and 480 eV show the Auger lines for carbon, nitrogen and oxygen atoms, respectively. As the cross section decreases with increase in emission angles, the peaks get sharper. The blue solid lines and red dash-dotted lines show the CDW-EIS calculations for BrU and uracil respectively. The model shows a qualitative agreement with the experimental data. The position of the binary encounter peak is also estimated accurately by the model. Quantitatively the model underestimates the data points for either targets. At 20° (see Figure 7.7(a)), the model calculations for uracil matches with the experimental points beyond 250 eV but underestimates the data in the low energy regime. For the same emission angle, the CDW-EIS calculations for bromouracil underestimates the measurements over the entire emission energy range. Similarly at 45° , the deviation from the experimental data points decreases beyond 200 eV. However, the deviations between the calculations and the data points increases further with the increase in emission angles. In case of the backward angles it is seen that the model predictions are in close agreement with the measured DDCS for uracil at the low electron energies and then underestimates the data beyond 30 eV. For bromouracil, the calculations predict lower cross section values for the lowest energy electrons at the backward angles. For example, at 105° (see Figure 7.7(e)), the model underestimates the data by 1.2 times at 10 eV which increases

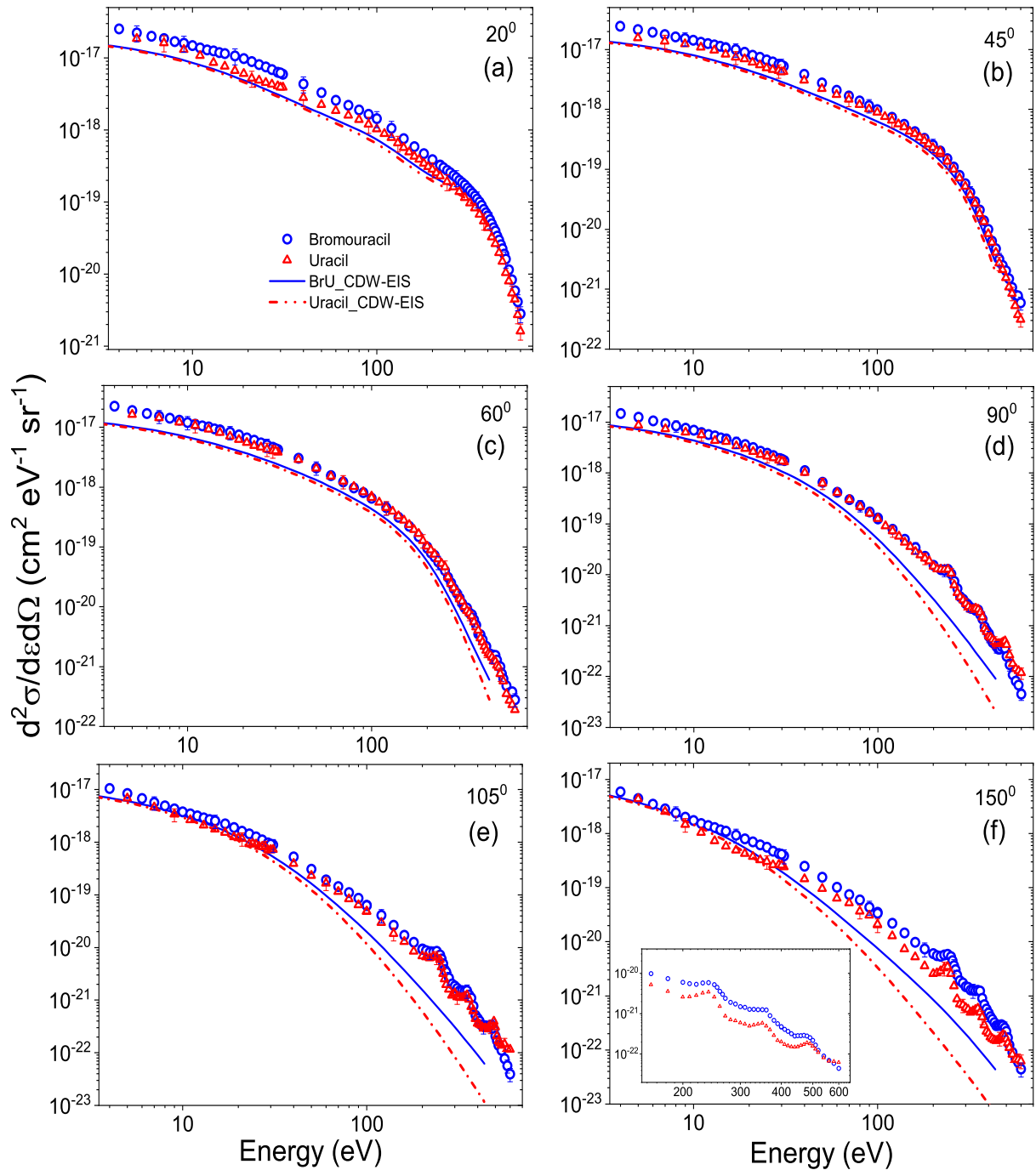


Figure 7.7: Absolute electron DDCS at fixed emission angles for 200 keV proton impact on bromouracil (blue open circles) and uracil (red open triangles). Inset of panel (f) show the K-LL Auger peaks for carbon, nitrogen and oxygen. The blue solid and red dash-dotted lines show the CDW-EIS predictions for bromouracil and uracil, respectively. The total absolute error bars are shown for some data points for both the target molecules.

to 3.84 times at 140 eV. Similar behaviour is also observed in case of the extreme backward angles.

7.5.2 DDCS ratios of bromouracil to uracil

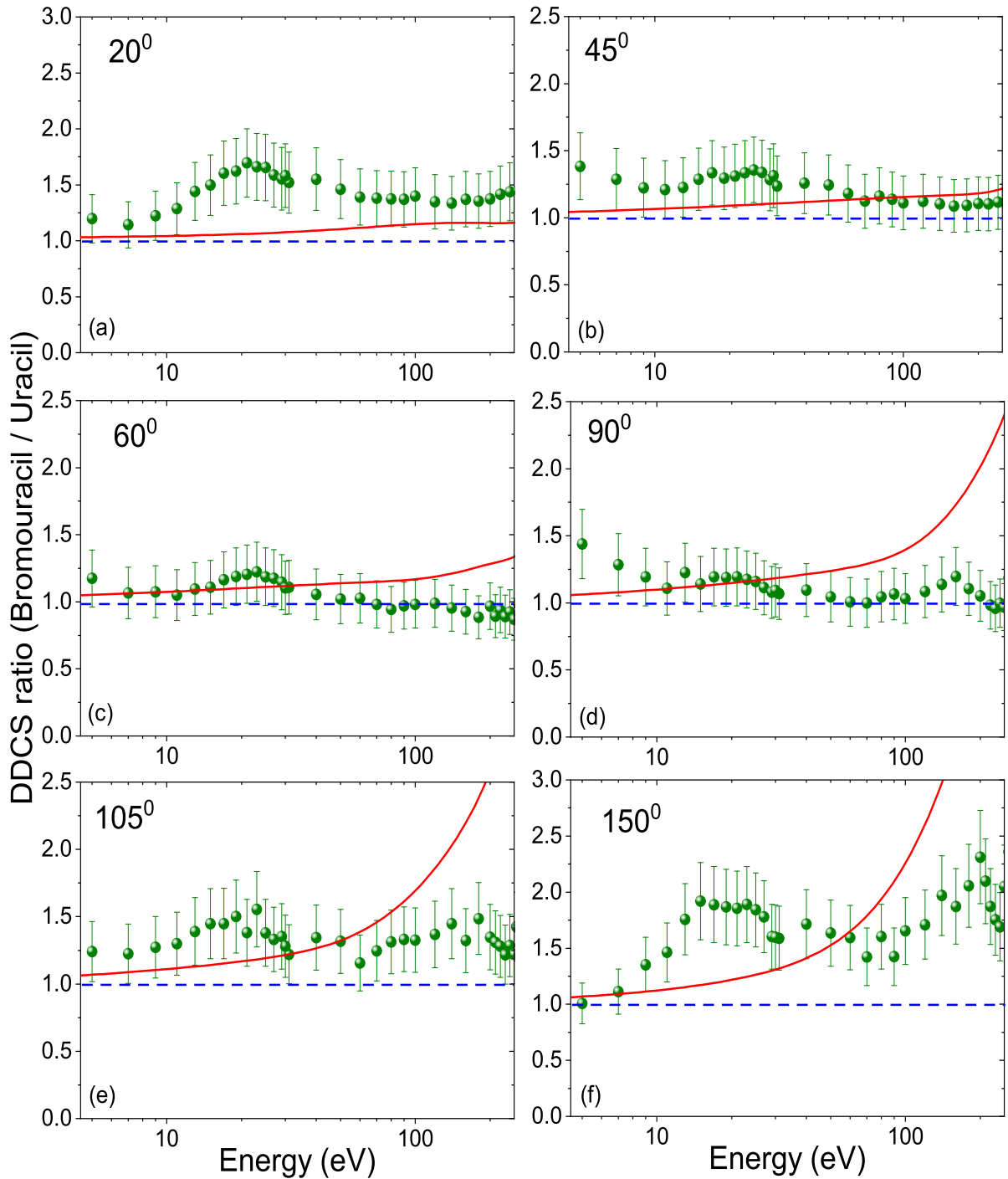


Figure 7.8: Ratio of DDCS between bromouracil and uracil for different emission angles; Projectile : 200 keV protons. The red solid line shows the DDCS ratio obtained from CDW-EIS calculations. Blue dashed line represent the ratio value at 1.0.

In [Figure 7.8](#) we have shown the ratio in the ionization cross section from bromouracil to that for uracil in collisions with 200 keV protons. The ratios have been plotted for six emission

angles comprising of forward and backward ones. These ratios are plotted to understand the exact difference in ionization cross section between the two molecules when collided by the same projectile beam under the same experimental conditions. At 20° , the experimentally obtained DDCS ratios show that the cross section for BrU is 1.2 to 1.7 times higher than the cross section for uracil. At the lowest electron energies the DDCS for BrU is 1.2 times higher which gradually increases upto 1.7 times and then again falls, showing an average enhancement of about 1.4 times at 20° . The theoretical ratios represented by the red solid line shows an enhancement by a factor of 1.15 times for emission energies above 100 eV, in case of the same emission angle 20° . The blue dashed line shown in all the panels represent the DDCS ratio for 1.0. However, in case of the other forward angles (i.e., 45° , 60° and 90°), the experimental ratios reveal a slightly different behaviour than that observed at 20° . For these angles, it is seen that the experimental ratios vary between 1.1 and 1.4 and for some cases the ratios are just below 1.0. The theoretical ratios are seen to match mostly with the experimental ratios at 45° and 60° within experimental uncertainties. At 90° , the CDW-EIS predicts a sharp rise in the DDCS ratio after 40 eV. As far as the theoretical ratios are concerned, similar behaviour is observed even at the backward angles. The experimental ratios show that on an average the DDCS for bromouracil is ~ 1.4 times higher than uracil for 105° and this factor goes up to 1.7 times for 150° emission angle. As already stated in case of 5.5 MeV/u C^{6+} ions, the DDCS ratios are generated to obtain a quantitative estimate of the enhancement in low energy electron production from BrU compared to uracil due to the presence of the Br atom. In case of 200 keV protons, due to the strong post collision interactions in the forward angles which gives rise to high cross sections for both uracil and bromouracil, it is difficult to estimate the enhancement due to Br atom. At these forward emission angles, the Auger effects are completely shadowed by the two center effect and post collisional interactions and hence it is difficult to predict the contribution from Auger cascade or GDR due to Br atom. For the present projectile beam, the enhancement from the experimental studies at the backward angles may be considered to provide an accurate understanding of the enhancement in electron emission from the halouracil.

7.6 Forward-backward angular asymmetry

Following the prescription of Fainstein *et al*[109], the forward-backward angular asymmetry parameter ($\alpha(k)$) is defined as:

$$\alpha(k, \theta) = \frac{\sigma(k, \theta) - \sigma(k, \pi - \theta)}{\sigma(k, \theta) + \sigma(k, \pi - \theta)} \quad (7.6)$$

here the electron energy $\epsilon_k = \frac{k^2}{2}$ in a.u., θ is a low forward angle and k denotes the ejected electron velocity. The angular distribution vary slowly near 0 and π , and hence the measured DDCS at 20° or 30° was used to calculate the approximate value of the asymmetry parameter.

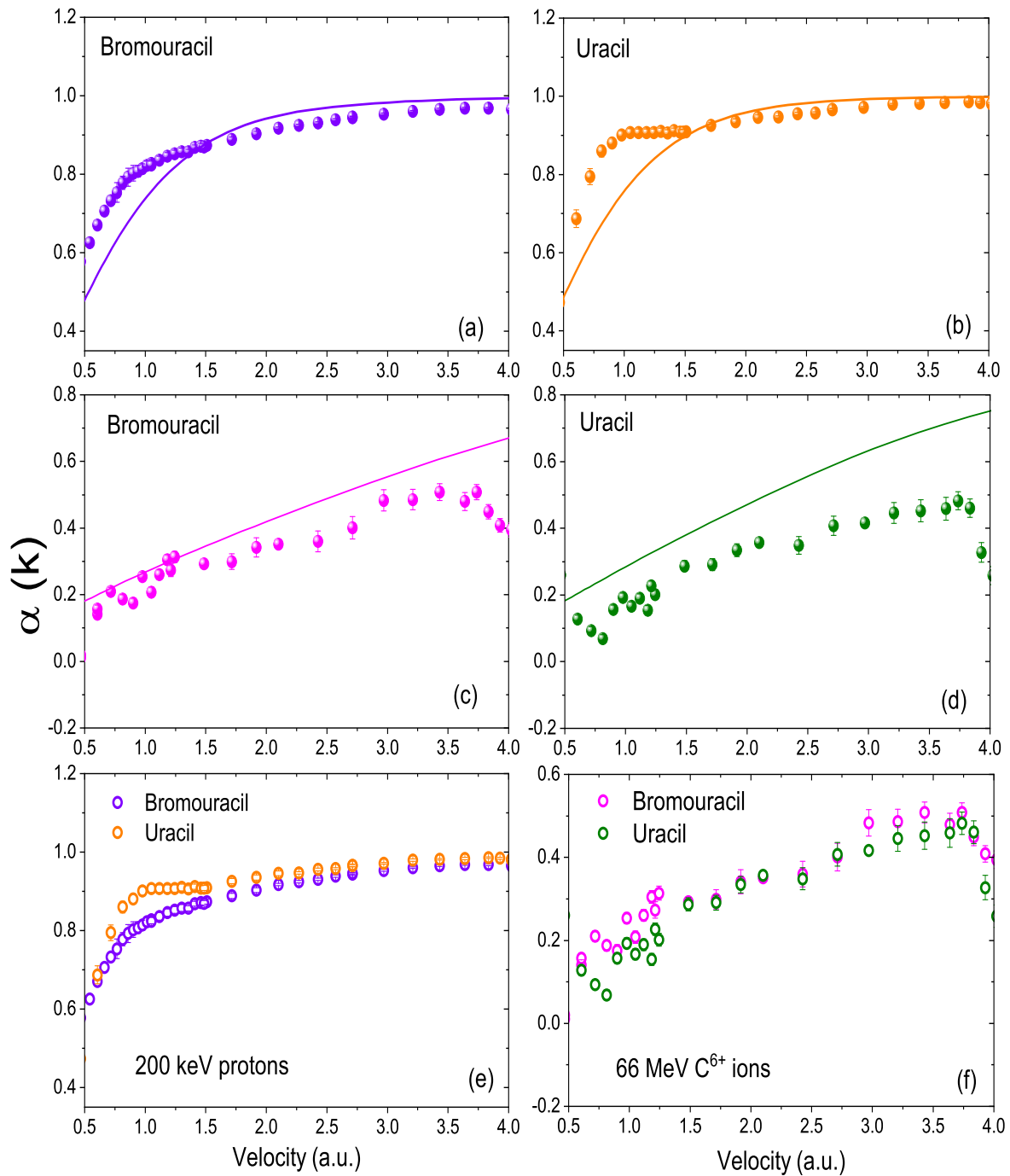


Figure 7.9: Asymmetry parameter ($\alpha(k)$) for different collision systems under investigation : (a) 200 keV H^+ + BrU (b) 200 keV H^+ + Uracil (c) 5.5 MeV/u C^{6+} + BrU (d) 5.5 MeV/u C^{6+} + Uracil. The solid lines in all the four panels represent the $\alpha(k)$ values obtained from the CDW-EIS calculations. Panels (e) and (f) show the experimentally obtained $\alpha(k)$ values of BrU and uracil plotted together for 200 keV protons and 66 MeV bare C ions, respectively.

In case of 5.5 MeV/u bare C ions colliding with BrU and uracil, the DDCS at 20° and 160° were used to obtain the forward-backward angular asymmetry. Similarly, for 200 keV proton impact

ionization studies, the cross section at 30° and 150° were used to derive the asymmetry parameter for uracil and bromouracil. Figure 7.9 display the forward-backward angular asymmetry for uracil and bromouracil in collisions with 5.5 MeV/u bare C ions and 200 keV protons. In panels (a) and (b) of Figure 7.9, it is seen that a large asymmetry exists for bromouracil and uracil when collided with 200 keV protons. The experimentally obtained $\alpha(k)$ values for bromouracil are seen to increase monotonically from 0.6 to 1.0 over the electron velocity of 0.5 to 4.0 a.u. The CDW-EIS model predicts similar kind of behaviour varying from 0.5 to 1.0. The asymmetry parameter for uracil in collisions with 200 keV protons (Figure 7.9(b)) shows similar behaviour to that seen for bromouracil. For either cases, although theory shows a qualitative agreement with the experimentally obtained $\alpha(k)$ values, but it is noted that for electron velocities upto about 1.5 a.u., experimentally obtained $\alpha(k)$ is larger than the model predictions. Around 1.5 a.u., there is a cross-over of the data points about the theoretical curve and thereafter the $\alpha(k)$ values predicted by CDW-EIS are higher than experimental data points. Both the theoretical calculations and measurements show a saturation effect in the asymmetry parameter beyond 2.75 a.u. To obtain a quantitative estimate of the difference in $\alpha(k)$ between the two target molecules when collided by the same projectile beam (i.e., 200 keV protons in the present case), we have plotted the experimentally determined $\alpha(k)$ for BrU and uracil together in Figure 7.9(e) as a function of electron velocity. Quantitatively it is observed that $\alpha(k)$ is larger for uracil compared to BrU in the lower electron velocity regime. This difference decreases as one goes higher in the electron velocity and finally around 2.75 a.u. and above, the two spectra tend to almost merge together. On the contrary, for 66 MeV bare C ions, $\alpha(k)$ shows a different character both experimentally and theoretically. The asymmetry parameter is much lower in the present case varying from 0.1 at the lowest electron velocities to about 0.4 for electron velocities of 4 a.u. (see Figure 7.9(c)). Similar behaviour is observed for uracil as well (Figure 7.9(d)). Here theory predicts higher $\alpha(k)$ values for both the target molecules with the deviation being more for uracil. The asymmetry parameter doesn't show any trend to saturate for the MeV energy bare C ions compared to that seen for 200 keV protons. Figure 7.9(f) shows the $\alpha(k)$ for BrU and uracil together in case of 66 MeV bare C ion impact ionization. Here the trend is different to that observed in Figure 7.9(e). In the present case it is seen that $\alpha(k)$ for BrU is relatively higher than uracil upto about 1.25 a.u., beyond which the data points for the two targets merge together completely upto 3 a.u., and thereafter the asymmetry in bromouracil is seen to be again slightly higher than uracil. The large asymmetry parameter for 200 keV proton impact study suggest that two centre effect and post collisional interactions are much stronger for 200 keV protons compared to the MeV energy projectiles giving rise to large forward-backward angular asymmetry.

7.7 Conclusions

In conclusions, we have performed DDCS measurements for ionization of uracil, a nucleobase of RNA and bromouracil in collisions with 5.5 MeV/u bare C ions and 200 keV protons. In case of bromouracil, measurements have also been extended for 3.5 MeV/u bare C ions. The DDCS measurements have been compared with the CDW-EIS calculations for both the projectiles at two different energy regimes. In almost all the cases it has been observed that theory predicts lower cross section than the measured DDCS. Further, the ratio of the DDCS for bromouracil to uracil were derived for all the emission angles for both 66 MeV C⁶⁺ ions and 200 keV protons. The ratios were deduced to understand quantitatively the enhancement in electron emission from bromouracil compared to uracil due to the presence of the Br atom. For 5.5 MeV/u bare C ions, an enhancement of approximately 1.25 times has been observed for majority of the emission angles. Similarly for 200 keV proton impact studies when performed on the same target species showed an enhancement of electron emission by a factor of about 1.4 to 1.5 times from bromouracil. In a similar kind of study reported recently [53], we have shown the DDCS for electron emission from iodouracil and uracil and it has been observed that the enhancement in electron emission from iodouracil is by a factor of about 2.3 times which is explained by the well known GDR feature present in iodine atom. As expected, the enhancement in electron emission from bromouracil should be less than that from iodouracil and our present experimental investigations fall in line showing an overall enhancement of about 1.4 times in case of bromouracil. This shows that addition of a single Br or I atom to a uracil molecule can increase the yield of the low energy electrons which are the main catalyst for radiation damage.